Geoscience Frontiers 10 (2019) 43–54

HOSTED BY

Contents lists available at ScienceDirect

China University of Geosciences (Beijing)

Geoscience Frontiers

journal homepage: www.elsevier.com/locate/gsf

Research Paper

Deformation at low and high stress-loading rates

Claudia A. Trepmann*, Lina Seybold

Department of Earth and Environmental Sciences, Ludwig-Maximilians University, Munich, Germany

ARTICLE INFO

Article history:
Received 1 November 2017
Received in revised form
19 March 2018
Accepted 11 May 2018
Available online 26 May 2018

Keywords:
High-stress crystal plasticity
Crack-seal
Seismic cycle
Stress-loading rates
Talea Ori
Crete

ABSTRACT

In an extensional shear zone in the Talea Ori, Crete, quartz veins occur in high-pressure low-temperature metamorphic sediments at sites of dilation along shear band boundaries, kink band boundaries and boudin necks. Bent elongate grains grown epitactically from the host rock with abundant fluid inclusion trails parallel to the vein wall indicate vein formation by crack-seal increments during dissolution-precipitation creep of the host rock. The presence of sutured high-angle grain boundaries and sub-grains shows that temperatures were sufficiently high for recovery and strain-induced grain boundary migration, i.e. higher than 300–350 °C, close to peak metamorphic conditions. The generally low amount of strain accumulated by dislocation creep in quartz of the host rock and most veins indicates low bulk stress conditions of a few tens of MPa on a long term. The time scale of stress-loading to cause cyclic cracking and sealing is assumed to be lower than the Maxwell relaxation time of the metasediments undergoing dissolution-precipitation creep at high strain rates (10^{-10} s^{-1} to 10^{-9} s^{-1}), which is on the order of hundred years. In contrast, some veins discordant or concordant to the foliation show heterogeneous quartz microstructures with micro-shear zones, sub-basal deformation lamellae, short-wavelength undulatory extinction and recrystallized grains restricted to high strain zones. These microstructures indicate dislocation glide-controlled crystal-plastic deformation (low-temperature plasticity) at transient high stresses of a few hundred MPa with subsequent recovery and strain-induced grain boundary migration at relaxing stresses and temperatures of at least 300–350 °C. High differential stresses in rocks at greenschist-facies conditions that relieve stress by creep on the long term, requires fast stress-loading rates, presumably by seismic activity in the overlying upper crust. The time scale for stress loading is controlled by the duration of the slip event along a fault, i.e. a few seconds to minutes. This study demonstrates that microstructures can distinguish between deformation at internal low stress-loading rates (to tens of MPa on a time scale of hundred years) and high (coseismic) stress-loading rates to a few hundred MPa on a time scale of minutes.

1. Introduction

Rocks correspond to stress by deformation. The stress conditions and their evolution with time in the lithosphere are of vital interest for all geodynamic processes. Early works of Sibson (1977) and Scholz (1988) indicated that shear zones can be characterized as deep continuations of seismic active faults, where the affected rocks deform controlled by stress loading and stress relaxation during the seismic cycle. Especially quartz veins have been found to be able to record the deep response of changes in stress and fluid pressure related to the seismic cycle (Henderson and McCaig, 1996; Famin et al., 2004; Nüchter and Stöckhert, 2007, 2008; Birtel and Stöckhert, 2008; Fagereng et al., 2018). Characteristic deformation microstructures that form at transient high stresses and subsequent modification at low stresses below the seismogenic zone, i.e., the plastosphere sensu Scholz (2002), have been identified from the geological record (e.g., Küster and Stöckhert, 1999; Trepmann and Stöckhert, 2003; Trepmann et al., 2017) in combination with experimental vein quartz deformation (Trepmann et al., 2007; Trepmann and Stöckhert, 2013). In these studies, the inferred transient high stresses in the plastosphere have been explained by "external" stress loading from seismic faulting in the overlying upper crust (Ellis and Stöckhert, 2004; Ellis et al., 2006; Nüchter and Ellis, 2010, 2011). Yet, stress loading in the plastosphere can also be related to "internal" processes, for example ductile instabilities with strain hardening (e.g., Hobbs et al., 1986; White,

* Corresponding author.
E-mail addresses: claudia.trepmann@lmu.de, lina.seybold@lmu.de (C.A. Trepmann).
Peer-review under responsibility of China University of Geosciences (Beijing).

https://doi.org/10.1016/j.gsf.2018.05.002

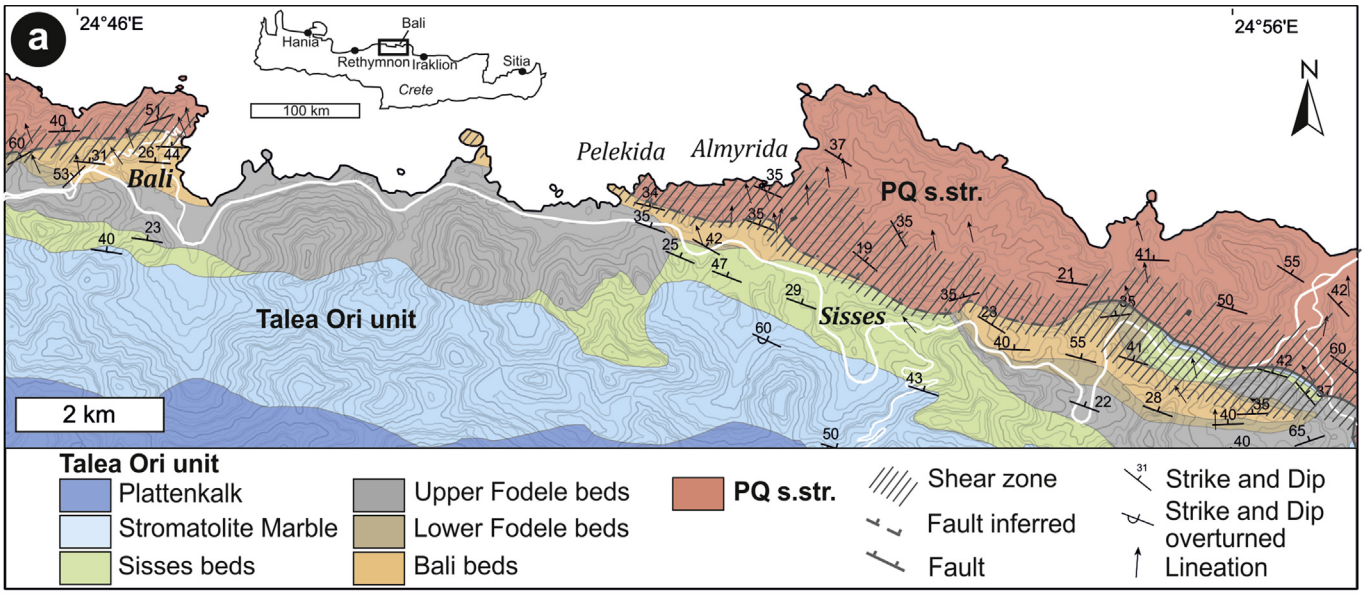

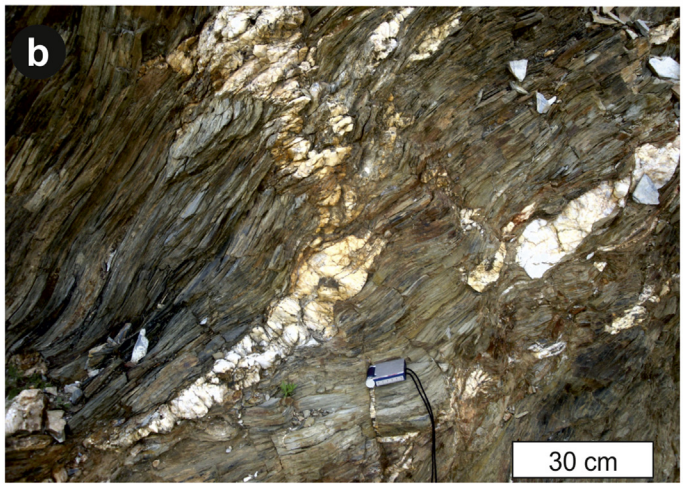

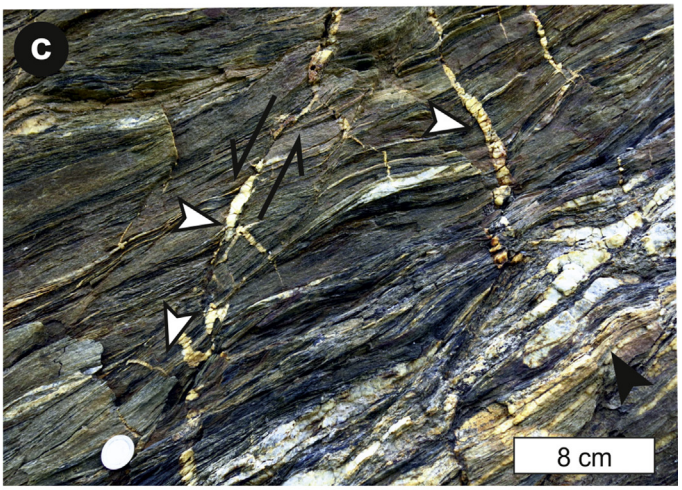

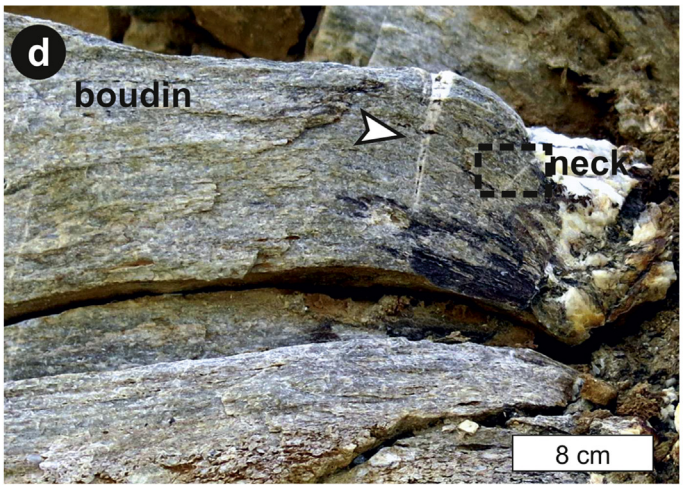

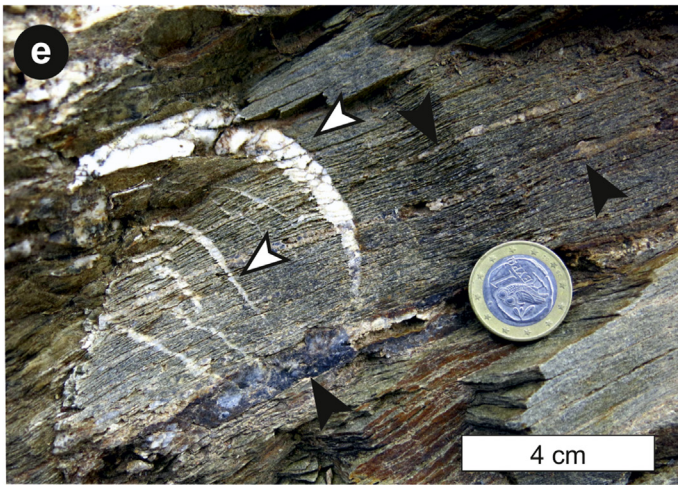

Figure 1. (a) Geologic map of the Talea Ori modified after Epting et al. (1972), Richter and Kopp (1983), and Kock et al. (2007). (b) Slaty cleavage of black shales in shear zone with quartz veins (Bali beds). (c) Extensional shear bands in schists with quartz precipitated along shear band boundaries (white arrows, PQ s.str.). Quartz veins concordant to the foliation are indicated by black arrow. (d) Quartzite boudin with a few cm-wide quartz vein in the boudin neck and mm-wide quartz veins (white arrow). Thin section micrographs from this sample, MB2 (PQ s.str.), are shown in Fig. 2a, f (dashed line). (e) Array of bent wedge-shaped discordant quartz veins (white arrows, PQ s.str.). Black arrows indicate quartz veins concordant to the foliation.

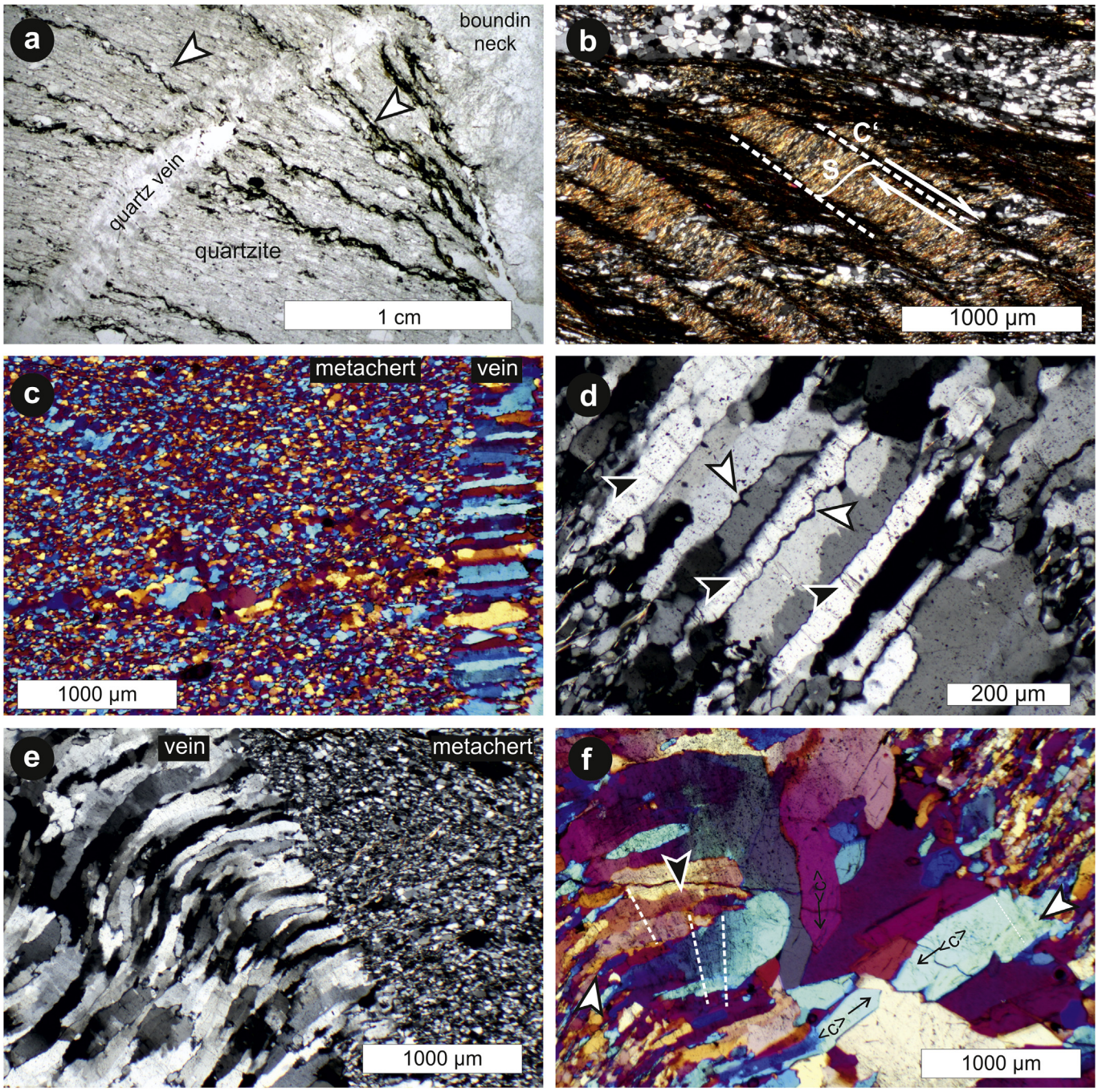

Figure 2. (a) Transmitted light micrographs of quartz vein in quartzite boudin displayed in Fig. 1d (dashed line), sample MB2 (PQ s.str.). The distance between layers enriched in opaque phases decreases towards the boudin neck (arrows). (b) Polarized light micrograph (crossed polarizers) showing shear band cleavage (C′-type) in black shale at Bali harbour (sample LS82). (c) Metachert and vein with elongate quartz grains of type A microstructure (crossed polarizers, compensator plate, sample LS128, Bali beds). Note that the optical characteristics do not reveal a CPO in the metachert. (d) Polarized light micrograph (crossed polarizers, sample LS128, Bali beds) of type A quartz vein microstructure characterized by elongate grains and fluid inclusion trails subparallel to the vein wall (black arrows). White arrow marks sutured grain boundaries. (e) Polarized light micrograph (crossed polarizers, sample LS128, Bali beds) of type A quartz vein microstructure. Note bent elongate grains, indicating growth during deformation of the host rock. (f) Polarized light micrograph (crossed polarizers, compensator plate, sample MB2, PQ s.str.) with type A microstructure close to the vein wall. In the centre of the vein, grains with rational boundaries are marked by the orientation of the c-axis. These grains are poor in fluid inclusions and show no undulatroy extinction, characterising the type B microstructure.

1996, 2012). Local stress concentrations can occur in high-viscosity particles in a low-viscosity matrix during boudinage and folding (e.g., Masuda et al., 1989; Trepmann and Stöckhert, 2009; Peters et al., 2016). Dehydration reactions during metamorphism have recently been described to result in quartz vein formation along the deep, tremorgenic subduction interface (Fagereng et al., 2018). Stress concentrations in the plastosphere by such internal processes lead to enhanced strain rates, which might load the seismogenic zone. Resulting earthquakes can again reload the plastosphere, which is characterizing the seismic cycle (e.g., Scholz, 2002). Here, we address the question, whether the microstructural record can distinguish between external stress loading of the plastosphere related to seismic activity in the upper crust and internal stress loading related to enhanced flow within the

plastosphere. We present quartz microstructures in veins of HP-LT metamorphic sediments from the Talea Ori, Crete, which are interpreted to reflect deformation at different stress-loading rates. We propose that the recorded rapid loading to high stresses requires external coseismic stress loading, whereas slow stress loading rates resulted from high strain-rate dissolution-precipitation creep.

2. Talea Ori, Crete

The island of Crete is situated in the forearc of the active Hellenic subduction zone. During collision of a microcontinent belonging to the African Plate with the southern margin of the Eurasian Plate in mid-Miocene times, parts of the sedimentary cover of the microcontinent were buried to high pressure-low temperature (HP-LT) metamorphic conditions (e.g. Fassoulas et al., 1994; Jolivet et al., 1996; Seidel et al., 2007; Ring et al., 2010). The HP-LT metamorphic rocks were rapidly exhumed from maximum burial depth of about 30–35 km between 24 Ma and 19 Ma to less than 10 km in depth before ca. 17 Ma (Thomson et al., 1998, 1999). In the Talea Ori at the northern central coast of Crete, Miocene HP-LT metamorphic rocks of the Talea Ori unit and the Phyllite-Quartzite unit *sensu stricto* (PQ s.str.) are exposed (Fig. 1a; e.g., Epting et al., 1972; Richter and Kopp, 1983; Kock et al., 2007; Trepmann et al., 2010; Zulauf et al., 2016). Peak metamorphic conditions indicated by petrological constraints are about 0.9 GPa and 350–400 °C for the Talea Ori in central Crete (e.g., Seidel et al., 1982; Theye et al., 1992), corresponding to burial depth of about 30 km. Raman spectroscopy of carboniferous material from the metasediments in the Talea Ori give a consistent temperature range of 350–430 °C (Rahl et al., 2005). The metasediments of the Talea Ori unit at the shear zone contact to the PQ s.str., the Bali beds, comprise a metaturbiditic sequence of black shales, metasandstones, quartzites, quartz metaconglomerates and metacherts (Fig. 1; Kock et al., 2007, Trepmann et al., 2010). The PQ s.str. is mainly composed of black albite schists, albite gneisses and quartzites (e.g., Zulauf et al., 2016).

3. Methods

Rock samples were collected on field campaigns between 2015 and 2017. Thin sections for transmitted light microscopy were prepared perpendicular to the foliation and parallel to the lineation. Sections used for analyses by electron backscatter diffraction (EBSD) at a scanning electron microscope (SEM) were polished by an alkaloid colloidal suspension (Syton) and coated with carbon. A field emission SEM (SU5000, Hitachi) equipped with EBSD facilities (NordlysNano Detector) at Ludwig-Maximilians University Munich, Department of Earth and Environmental Sciences, was used. An acceleration voltage of 20 kV and a working distance of 20–25 mm were applied on samples tilted at an angle of 70° with respect to the beam. EBSD patterns were automatically measured (step size of 0.7–1 μm) with the AZtec software (Oxford Technology) and post-processed using the software CHANNEL 5 (Oxford Technology). To present crystallographic orientations of the grains, stereographic projections of the lower hemisphere are used. The software also provides information about grain size and shape. For grain detection, a threshold value of 10° for the misorientation angle was used. The misorientation of silicates may be $> 10°$ (White, 1977). However, a higher threshold value of e.g. 15° did not change our results. Grain size is given as the diameter of a circle of equal area. TEM samples were prepared by ion thinning (GATAN PIPS) of 30 μm thin sections glued onto a copper grid. The TEM samples were thinned at voltages of 3–4 kV and an Ar-beam at an angle of 6°–8° with respect to the sample. TEM samples were analysed using bright field conditions at a Tecnai G2 (FEI) microscope operated at 200 kV at Ludwig-Maximilians University Munich, Department of Chemistry.

4. Results

4.1. Deformation structures and quartz veins

The deformation structures in the shear zone at the contact between the PQ s.str. and the Talea Ori unit include extensional shear bands, shear band cleavages, kink bands and boudins (Figs. 1b–e, 2a, b). Quartz veins discordant to the foliation and with a relative high ratio of aperture to length (typically around 1:6 to 1:10) are associated to these structures. Such aperture-to-length ratios exceed the elastic limit of fracture aperture, indicating that inelastic host rock deformation contributed to relief stresses concentrating at the fracture tips to keep the fracture arrested during aperture growth (e.g., Vermilye und Scholz, 1995; Olson, 2003). This is consistent with the relation of the quartz veins to ductile deformation structures of the host rocks, i.e. shear bands, boudins and kink bands within the shear zone (Fig. 1b–e). An older generation of quartz veins is concordant to the foliation (Fig. 1c, e). Discordant wedge-shaped quartz veins can occur in arrays (Fig. 1e). The quartz veins can contain minor amounts of albitic feldspar and chlorite may be present. In quartzites, the spacing between the foliation, characterized by layers rich in opaque minerals and mica, decreases towards quartz-sealed boudin necks (Fig. 2a). This microstructure indicates a relative enrichment of insoluble minerals caused by selective dissolution of quartz at sites of shortening, indicating dissolution-precipitation creep. In mica-rich layers of metasandstones and shales, C′-type shear band cleavage, also referred to as extensional cleavage (e.g., Platt and Vissers, 1980; Passchier and Trouw, 2005, Chapter 5.6.3), is common (Fig. 2b). The shear band cleavage is characterized by a passive enrichment of micas and opaque minerals, whereas quartz has been removed by dissolution, indicating dissolution-precipitation creep. At the sites of dilation, quartz is precipitated forming the observed quartz veins discordant to the cleavage, resembling an asymmetric foliation boudinage (Platt and Vissers, 1980). The metasediments generally show a shape preferred orientation (SPO) but no crystallographic preferred orientation (CPO) (Fig. 2a, c), revealing a low amount of strain accumulated by dislocation glide. These microstructures indicate vein formation by fracturing and sealing during dissolution-precipitation creep of the host rock.

4.2. Vein quartz microstructures

Three types of vein quartz microstructure are distinguished by the recorded strain and are presented in the following.

The ***type A microstructure*** is exclusively present in quartz veins discordant to the foliation (Fig. 2c–e). It is the most common vein microstructure. Elongate to blocky grains with long axes perpendicular to the vein wall characterize it. The crystallographic orientation of the grains indicates epitactic growth from the vein wall (Fig. 2c–f). Common fluid inclusion trails subparallel to the vein wall represent healed microcracks (Fig. 2d, f). This microstructure is characteristic of stretching veins, indicating formation by multiple crack-seal increments (e.g., Durney and Ramsay, 1973; Ramsay, 1980; Cox and Etheridge, 1983; Fisher and Byrne, 1990; Fisher and Brantley, 1992; Fisher et al., 1995; Nollet et al., 2005; Bons et al., 2012). Along the vein boundaries, the foliation in the host rock can be displaced (Fig. 1c). The curved shape of elongate grains is commonly not corresponding to a respective change of crystallographic orientation (Fig. 2e), indicating that they grew epitactically during deformation of the host rock, instead of being deformed after growth. Such bent elongate quartz grains can track

the shear-offset during vein widening (Durney and Ramsay, 1973; Ramsay and Huber, 1983; Urai et al., 1991). Yet, some crystal-plastic deformation and strain-induced grain-boundary migration after growth are indicated by the presence of undulatory extinction and sutured high-angle grain boundaries (Fig. 2d–f). TEM investigations show tiny grains with diameter of a few μm, abundant fluid inclusions along grain boundaries, a relative low free dislocation density and common low angle grain boundaries (Fig. 3a–c).

The ***type B microstructure*** occurs in the centre of veins discordant to the foliation, showing otherwise a type A microstructure at the area close to the vein wall. Towards the centre of these veins, grain sizes can increase, indicating growth competition of the fast growth direction parallel to the quartz c-axis (e.g., Durney and Ramsay, 1973; Fisher and Brantley, 1992; Fisher et al., 1995; Hilgers and Urai, 2002; Nollet et al., 2005; Bons et al., 2012). The type B microstructure is characterized by rational boundaries of quartz grains, representing crystallographic planes

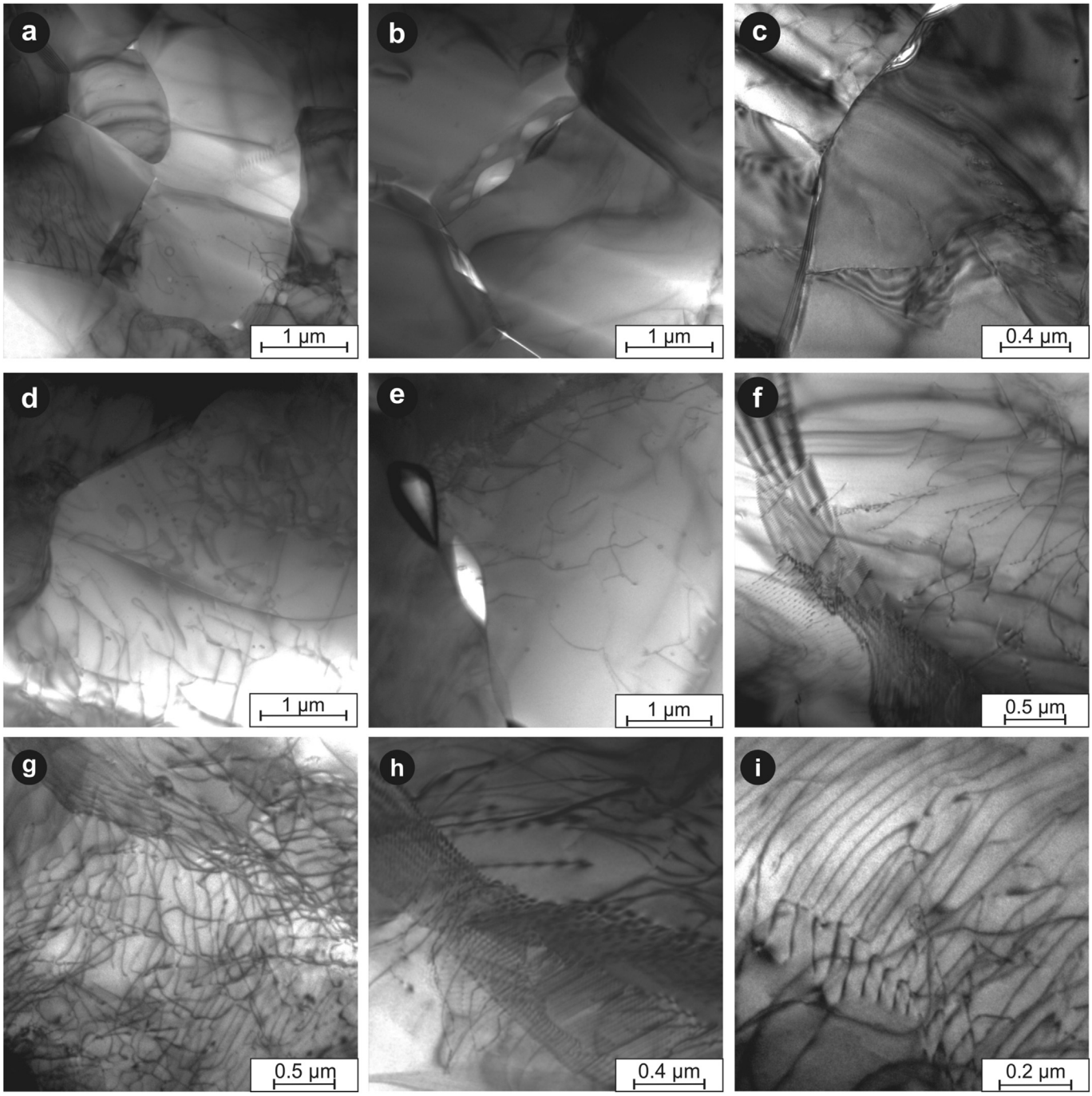

Figure 3. TEM bright field images of vein quartz from samples discordant to foliation. (a–c) Type A microstructure (sample MS 1, Bali beds, compare with Fig. 2e) showing new grains with low dislocation density, a high amount of fluid inclusions along grain boundaries and low angle grain boundaries. (d–i) Sample MB 1, PQ s.str. (type C microstructure, compare Fig. 6). (d) Curved high angle grain boundaries in grains with high dislocation density. (e) Fluid inclusions along high-angle grain boundary. (f–i) Low-angle grain boundaries and networks of tangled dislocations.

(Fig. 2f). These hypidiomorphic quartz grains are almost devoid of fluid inclusions and internal deformation structures as undulatory extinction and sutured grain boundaries, in strong contrast to the type A microstructure. The hypidiomorphic quartz crystals are elongate, with their long axis parallel to the c-axis, consistent with the quartz c-axis being the fast growth axis and growth in open cavities (Fisher and Brantley, 1992; Ague, 1995; Nollet et al., 2005). Consistently, associated veins can be partly open.

The heterogeneous ***type C microstructure*** can occur in the old generation of quartz veins concordant to the foliation of the host metasediments (Figs. 4 and 5) and rarely also in the young discordant veins associated to shear bands (Fig. 6). Sub-basal deformation lamellae, a marked short-wavelength undulatory extinction (SWUE) and micro-shear zones in conjugate sets (Figs. 4–6) characterize the type C microstructure. Deformation lamellae sub-parallel to the basal plane can occur in concordant veins and in host rocks (Fig. 4c, d). They show a slight difference in refractive index and a low oscillating change in misorientation angle of $<1^\circ$ at the detection limit of the EBSD technique. Such sub-basal deformation lamellae are common in quartz deformed at high stresses and greenschist facies conditions (e.g., McLaren et al., 1970; McLaren and Hobbs, 1972; White, 1973, 1977; Christie and Ardell, 1974; Drury, 1993; Trepmann and Stöckhert, 2003, 2013). An oscillatory change in misorientation angle of a few degrees is characterizing the SWUE (Fig. 5a, e). Along micro-shear zones, the orientation abruptly changes with misorientation angles being generally smaller than 10° (Fig. 5a, e). The micro-shear zones in conjugate sets are sub-parallel to one {r} and one {z} rhombohedral planes of the host orientation (Figs. 4b and 5a, c). They show a systematic difference in crystallographic orientation, indicating a dextral or sinistral rotation of the c-axes with respect to the host orientation in micro-shear zones parallel to the {z} and {r} planes, respectively (Figs. 4b and 5a, e). The angle between the c-axes in the micro-shear zone and the host grain is with in average 5° very similar in both sets of micro-shear zones. Similar conjugate micro-shear zones with systematically different crystallographic orientations are described for example by Van Daalen et al. (1999), Kjøll et al. (2015), Ceccato et al. (2017) and Trepmann et al. (2017), where both brittle and crystal-plastic mechanisms are discussed to be involved in their formation. Dauphiné twin orientations are common along the micro-shear zones (Fig. 5a–c). Mechanical Dauphiné twinning of quartz is observed in quartz mylonites (e.g., Pehl and Wenk, 2005; Wenk et al., 2006, 2011; Kjøll et al., 2015). Dauphiné twin boundaries can be modified during recrystallization of quartz, resulting in HAGBs with large misorientation angles (Lloyd, 2004; Menegon et al., 2011). Most new grains (about 70%) in micro-shear zones have diameters of smaller than 8 μm, as indicated by EBSD-measurements (Fig. 5b, d, f). Recrystallized grains can also occur restricted to high angle grain boundaries or intragranular cracks (Fig. 6b, d, e). There, most new grains (ca. 70%) have a grain diameter smaller than 10 μm with an expected value of 9 μm (Fig. 6e). Subgrains similar in shape and size are common close to recrystallized areas (Fig. 6c). New grains show similar grain orientations as the deformed host (Fig. 6g, f). TEM observations of quartz from the vein in Fig. 6 show high dislocation densities (Fig. 3d–i). Sutured high angle grain boundaries (Fig. 3d) and grain boundaries decorated by fluid inclusions (Fig. 3e), as well as low angle grain boundaries (Fig. 3f, h) are common.

5. Discussion

The three different types of vein quartz microstructure are interpreted to represent deformation at different stress conditions, which is discussed in the following.

5.1. Growth of quartz in open cavities at quasi-isostatic stress conditions

The ***type B microstructure*** with hypidiomorphic grains and no internal deformation microstructures, exclusively occurring in

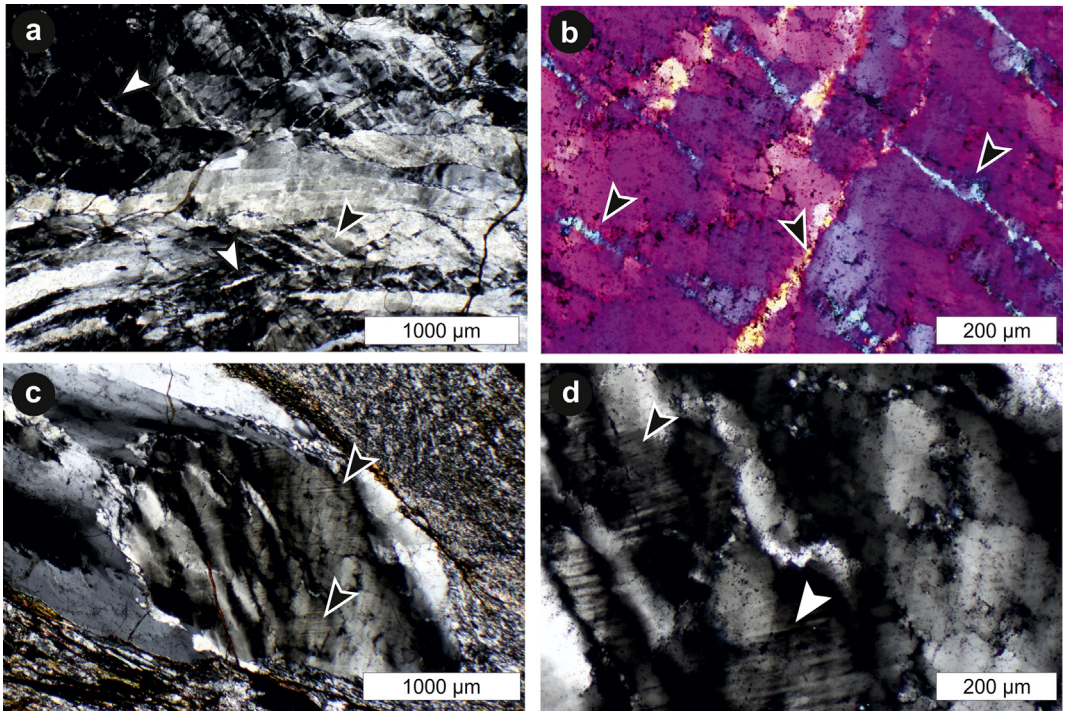

Figure 4. Transmitted light micrographs with crossed polarizers of vein quartz microstructure type C revealing high stress, dislocation glide-controlled deformation. (a) Vein quartz concordant to the foliation showing elongate grains and micro shear zones, in conjugate sets (arrows) (CT83). (b) Close-up of micro-shear zones. Micrograph is taken with compensator plate inserted, indicating systematic rotation of the quartz c-axes with respect to the host orientation (sample LS12 Bali beds, compare with Fig. 5). (c, d) Quartz vein showing short wavelength undulatory extinction and deformation lamellae (black arrows, LS12, Bali beds).

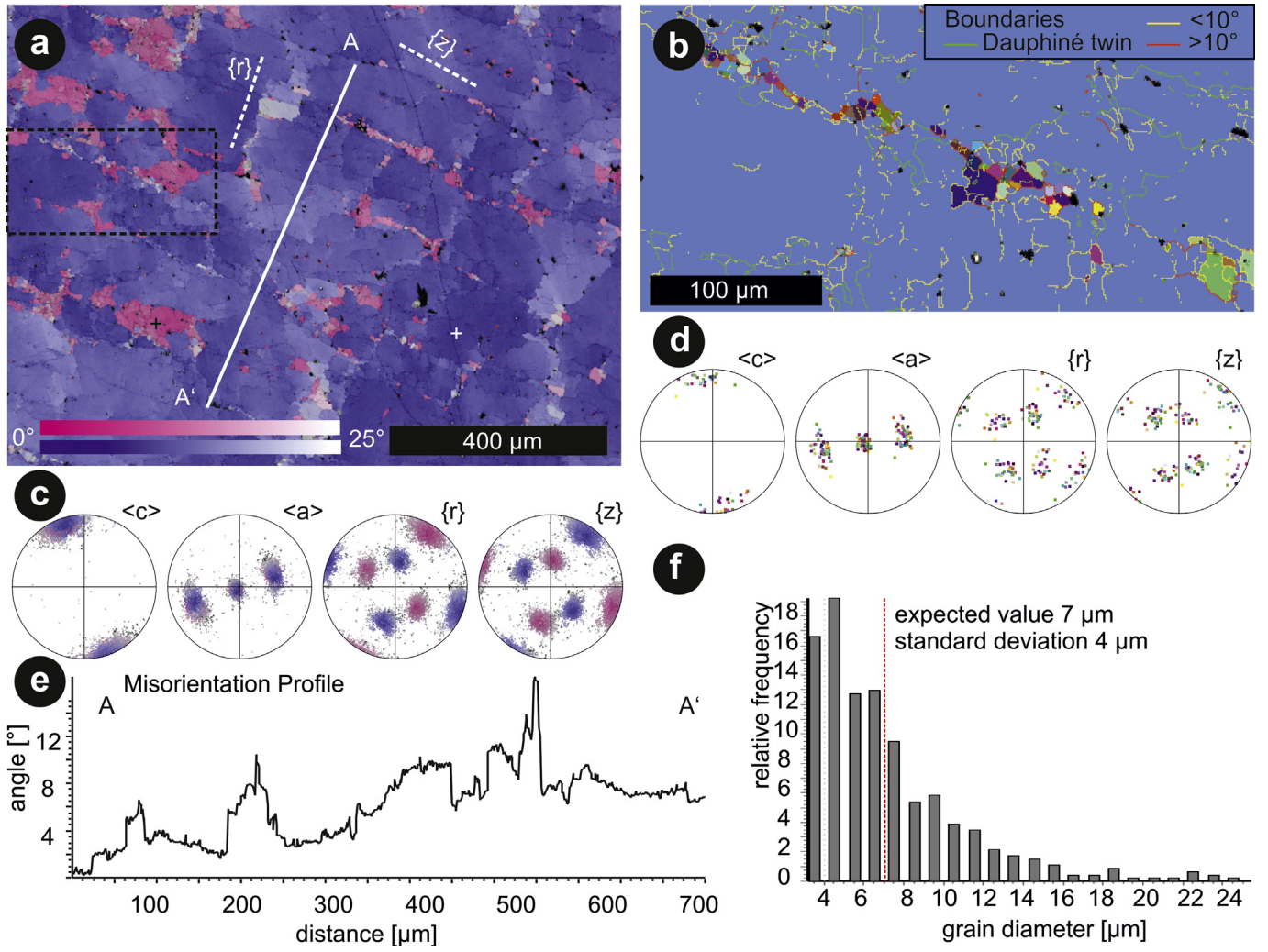

Figure 5. EBSD data of optical microstructure shown in Fig. 4b (sample LS12). (a) EBSD map, colour coding is by misorientation angle of up to 25° to a reference orientation of the host grain (white cross) and Dauphiné twin domains (black cross). Host orientations are in dominating blue colour, Dauphiné twins in red colour (compare with Fig. 5c). Orientation of misorientation profile (AA′) is indicated by white line. Dashed white lines indicate traces of one {r} and one {z} rhombohedral plane (compare with Fig. 5c). Black dashed box indicates close-up in (b). (b) Close-up of a micro-shear zone with new grains in random colours (neglecting Dauphiné twins). Grain boundaries are indicated by yellow (low-angle grain boundaries with misorientation angle <10°) and red lines (high-angle grain boundaries with misorientation angle >10°). (c) Corresponding pole figures, stereographic projection of the lower hemisphere. (d) Corresponding polefigures for new grains (one point per grain). (e) Misorientation profile to line displayed in (a). (f) Grain size distribution for new grains.

discordant quartz veins, represents the latest stage of veining, after which the temperature-stress conditions were too low to allow for crystal-plastic deformation of quartz. The rational grain boundaries together with the associated partly open fractures indicate that vein opening was fast compared to the precipitation rates (e.g., Fisher and Byrne, 1990; Fisher and Brantley, 1992; Ague, 1994, 1995; Fisher et al., 1995; Hilgers et al., 2003; Nollet et al., 2005). This suggests that ductile deformation of the host rocks by dissolution-precipitation creep was ongoing, forming the cavities. The fluid pressure remained high enough to keep the veins open against the lithostatic pressure. These microstructures indicate that stresses relaxed and became quasi-isostatic after precipitation of the crystals into the residual cavities and completion of the veins.

5.2. *Vein formation by crack-and-seal increments – deformation at low stress-loading rates*

The curved shape of elongate grains characteristic of the ***type A microstructure***, which is not corresponding to a change of crystallographic orientation (Fig. 2e and f), indicates deformation of the host rock during sealing (Durney and Ramsay, 1973; Ramsay and Huber, 1983; Urai et al., 1991). The elongate grains epitactically growing from quartz grains in the host rock with healed microcracks parallel to the vein wall indicate formation by crack-seal increments, where the average vein opening velocity is smaller than the growth velocity of the crystals as indicated from numerical simulation (e.g., Hilgers et al., 2001; Nollet et al., 2005). The observation that the crack-seal microstructures exclusively occurs in discordant veins located at sites of dilation along shear band boundaries, kink band boundaries and boudin necks (Fig. 1b–e) shows that vein formation by cracking and sealing is related to dissolution-precipitation creep of the metasediments.

Undulatory extinction, subgrains, sutured high-angle grain boundaries (Fig. 2c–f) and tiny dislocation-free new grains observed in TEM (Fig. 3a) indicate that most of the veins formed at temperatures sufficiently high to allow for dislocation climb and strain-induced grain boundary migration, i.e. temperatures of at least 300–350 °C. These temperatures are close to the peak

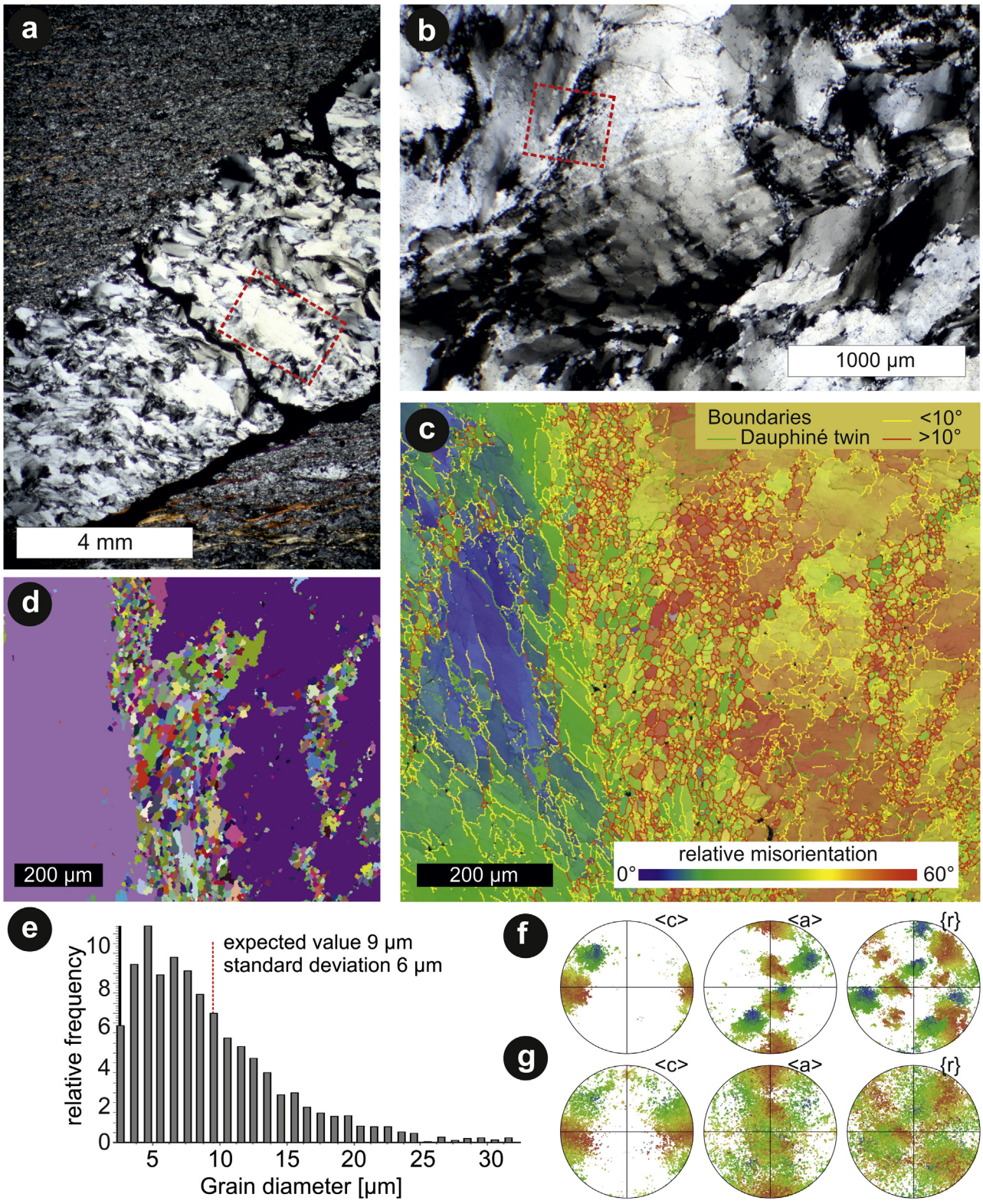

Figure 6. Type C quartz microstructure of vein discordant to foliation in metasandstone (sample MB1, PQ s.str.). (a, b) Cross polarized light micrographs showing short-wavelength undulatory extinction and localized zones of recrystallized grains. Box in (a) shows close-up photograph in (b), box in (b) is indicating area of the EBSD map in (c) and (d). (c) EBSD map with colour coding by relative misorientation angle (up to 60°) with respect to blue colour. Lines indicate Dauphiné twin boundaries (green), low-angle (yellow) and high-angle (red) grain boundaries. (d) EBSD map of same area showing new grains in random colours. (e) Histogram of grain sizes of new grains. (f, g) Lower hemisphere stereographic projection of host grains and new grains, respectively.

metamorphic conditions for the rocks of central Crete (about 0.9 GPa, 350 °C after Seidel et al., 1982; Theye et al., 1992). Given the extensional character of the shear bands and boudins, the veins formed most probable during exhumation from depth of maximal 30 km within the subduction channel.

The generally low amount of strain accumulated by dislocation creep of quartz in most veins and host rocks implies that stresses in these rocks were too low to result in relevant strain rates of dislocation creep at the given temperatures. Thus, flow laws for dislocation creep of quartz can be used as lower bound of the differential stress (e.g., Stöckhert, 2002; Trepmann and Stöckhert, 2009; Wassmann and Stöckhert, 2013). For temperatures of 300–350 °C and a strain rate of 10^{-15} s^{-1}, the flow law of Paterson and Luan (1990), equation (1), predicts differential stresses below a few tens of MPa.

$$d\varepsilon/dt = A \cdot \exp(-Q/RT) \cdot \sigma^n \quad (1)$$

with the parameters $A = 6.5 \times 10^{-8}$ MPa^{-n}/s; $Q = 135 \pm 15$ kJ mol^{-1}; $n = 3.1$.

Applying different creep parameters for a rheology controlled by dislocation creep of quartz (e.g., Ranalli, 1995, Chapter 10), yields the same order of magnitude. These differential stress conditions of less than few tens of MPa are consistent with the record of static recrystallization of quartz in HP-LT metamorphic conglomerates from related tectonic units in the Talea Ori (Trepmann et al., 2010). Generally, the record of rocks exhumed from subduction zones indicate low bulk stress conditions and a long-term rheology dominated by dissolution-precipitation creep over crystal-plastic deformation in subduction zones (e.g., Stöckhert et al., 1999; Wassmann and Stöckhert, 2013). Consistently, the expected brittle strength of the host rock at the given P-, T-conditions and the indicated high pore fluid pressures would not require higher stress conditions for the crack-seal processes.

As vein opening is related to dissolution-precipitation creep in the metasediments, the time interval for the crack-seal episodes depends on the effective viscosity of the metasediments. Dissolution-precipitation creep is a deformation mechanism, which allows for the accumulation of high strain at low bulk stress conditions characterized by relatively low viscosities on the order of 10^{19}–10^{20} Pa s (e.g., Trepmann and Stöckhert, 2009; Wassmann and Stöckhert, 2013). Considering a Maxwell rheology, the time required to dissipate the imposed stress can be expressed by the relaxation time λ_R (e.g., Ranalli, 1995, Chapter 4), which is defined as the viscosity (η) divided by the shear modulus, G (1).

$$\lambda_R = \eta/G \quad (2)$$

For viscosities, η, of 10^{19}–10^{20} Pa s and a typical shear modulus, G, for schists of 19 GPa (Johnson and DeGraff, 1998) it is on the order of a few tens to hundred years. The time scales of stress build up for cracking and sealing can be assumed lower than the Maxwell relaxation time of the metasediments undergoing dissolution-precipitation creep. Progressive vein formation might cause increasing bulk strength of the rocks, as veins represent high-viscosity layers in a low-viscosity matrix.

The Deborah number, *De*, relates relaxation time and the characteristic time of a deformation process (e.g., Poole, 2012). For our purpose, *De* can be considered as Maxwell relaxation time multiplied with strain rate, $d\varepsilon/dt$ (2).

$$De = \lambda_R \cdot d\varepsilon/dt \quad (3)$$

When *De* becomes >1, i.e. the Maxwell relaxation time is higher than the reciprocal of the strain rate, $d\varepsilon/dt$, the material cannot dissipate the imposed stress. Assuming a viscosity of 10^{19} Pa s for the metasediments undergoing dissolution-precipitation creep, a strain rate of 2.5×10^{-9} s^{-1} would be required for this critical behaviour, and 3.5×10^{-10} s^{-1} would be required for a viscosity of 10^{20} Pa s. Such high strain rates are predicted along the plate interface in subduction zones, which depend on relative plate velocity and cumulative shear zone width (e.g., Fagereng and Sibson, 2010). For a convergence of about 4.5 cm/yr for the Hellenic subduction zone (McClusky et al., 2000), and 10 m cumulative shear zone width, for example, the predicted strain rates are on the order of 10^{-10} s^{-1}.

5.3. High-stress dislocation glide-controlled deformation

The heterogeneous ***type C microstructure*** occurs sporadically in older vein generations concordant to the foliation (Figs. 4 and 5) and few young discordant veins related to the extensional shear zone (Fig. 6). Sub-basal deformation lamellae and SWUE (Figs. 4c, d, 5a, e and 6b) reflect high-stress dislocation glide-controlled deformation with subsequent modification by recovery (e.g., McLaren and Hobbs, 1972; Christie and Ardell, 1974; Drury, 1993; Trepmann and Stöckhert, 2003, 2013; Vernooij and Langenhorst, 2005). Micro-shear zones in conjugate sets (Figs. 4a, b and 5) involve brittle and crystal-plastic mechanisms with formation of new grains by nucleation and growth (Trepmann et al., 2007; Kilian and Heilbronner, 2017) associated with subgrain rotation and strain-induced grain boundary migration (Van Daalen et al., 1999; Ceccato et al., 2017; Trepmann et al., 2017) at greenschist facies conditions. In the type C microstructure, recrystallized grains are generally restricted to sites of localised high strain (i.e., along intragranular cracks and pre-existing grain boundaries, Figs. 5 and 6). Abundant low angle grain boundaries (Fig. 3e, f, h), subgrains of similar shape and size close to recrystallized grains (Fig. 6c) and new grain orientations scattering around the orientation of the host grain (Fig. 6f and g) indicate recrystallization with subgrain rotation and strain-induced grain-boundary migration (e.g., Stipp and Kunze, 2008; Ceccato et al., 2017; Trepmann et al., 2017). The sequence of dislocation glide-controlled and associated brittle deformation of quartz producing highly damaged zones, which are sites of subsequent formation of new grains is interpreted to reflect initially high and then relaxing stresses (Trepmann and Stöckhert, 2003; Trepmann et al., 2017), consistent to microstructures produced in deformation experiments at such stress histories (Hobbs, 1968; Trepmann et al., 2007). During high-stress dislocation glide-controlled deformation (low-temperature plasticity, Peierls stress-controlled glide), strain rates are too high at given temperature for effective concomitant dislocation climb, causing dislocation pile up with strain hardening and associated microcracking (e.g., Hobbs, 1968; Drury, 1993; White, 1996). The resulting localized high strain zones are sites of recrystallization during dislocation creep at subsequently relaxing stresses (e.g., Hobbs, 1968; Trepmann and Stöckhert, 2003; Trepmann et al., 2007, 2017).

Because of the transient nature of this deformation and relatively low strain, paleopiezometers are difficult to apply and they can at best record some arbitrary stage of stress relaxation after peak stresses (e.g., Trepmann and Stöckhert, 2003). However, at least as a very rough indicator of a lower stress bound, we can use the grain diameters of new grains in the micro-shear zones within the range of 7–10 μm (Figs. 5f and 6e). Following the paleopiezometer of Stipp and Tullis (2003), these grain diameters would indicate differential stresses within the given error range between 45 MPa and 400 MPa for the stage of recrystallization at already relaxed stresses. Initial dislocation-glide controlled deformation with the formation of deformation lamellae (Christie and Ardell, 1974; Drury, 1993; Trepmann and Stöckhert, 2003, 2013; Vernooij and Langenhorst, 2005), micro-shear zones (Trepmann et al.,

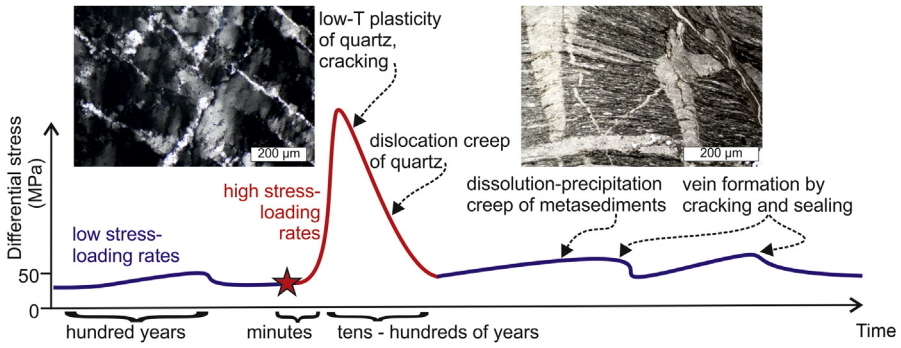

Figure 7. Conceptual sketch showing the stress history during deformation of the host rock, see text for discussion.

2017) and Dauphiné twins (e.g., Pehl and Wenk, 2005; Wenk et al., 2006, 2011; Kjøll et al., 2015) would consistently indicate stresses of a few hundred MPa.

5.4. High (coseismic) stress-loading rates

The dominating microstructures indicative of low-stress, high-strain dissolution-precipitation creep of the host rocks and type A and B vein quartz microstructures are in marked contrast to the type C microstructure indicating high-stress, glide-controlled deformation. To explain the locally present evidence of high stresses we discuss two possibilities:

(1) Stresses concentrated in monophase quartz layers representing high-viscosity layers in a low-viscosity matrix (e.g., Masuda et al., 1989; Trepmann and Stöckhert, 2009; Peters et al., 2016).

If this would be the case, the type C microstructure should be much more common and dependent on the strain accumulated within the metasediments. This, however, has not been observed: The type C microstructure is not as common as the type A microstructure and can occur in veins both, concordant and discordant to the foliation. As such, it is not directly related to the high strain-rate by dissolution-precipitation creep of the metasediments in contrast to the crack-seal deformation indicated by the type A microstructure.

(2) Stress-loading in the flowing metasediments occurred as consequence of seismic rupture in the overlying seismogenic zone (e.g., Sibson, 1977; Scholz, 1988; Scholz, 2002), as simulated in numerical models by Ellis and Stöckhert (2004) and Nüchter and Ellis (2010, 2011).

We argue that loading of the middle crust, which relieves shear stress by creep on the long term, to high differential stresses must be achieved rapidly, presumably by seismic activity in the overlying upper crust (Küster and Stöckhert, 1999; Trepmann and Stöckhert, 2003). Slow stress-built-up at the given temperatures and lithologies would result in high strain-rate dissolution-precipitation creep with type A crack-seal microstructures before reaching the stresses required for low-temperature plasticity of monophase quartz layers. During fast stress-loading rates, dissolution-precipitation creep of the metasediments cannot relax the stresses sufficiently fast, so that transient peak stresses can build up causing dislocation glide-controlled deformation and associated microcracking in the monophase quartz veins.

The time scale of stress loading is characterized by the duration of the slip event along a fault, i.e., a few seconds to minutes, depending on the size of the fault and the seismic event (e.g., Wald and Heaton, 1994). Unfortunately, the microstructures in the Talea Ori do not provide good constraints on the peak stresses for coseismic deformation. In metagranites from the Sesia zone, Western Alps, peak stresses at the base of the seismogenic zone were estimated based on mechanical twinning of jadeite to be about 0.5 GPa or even higher (Trepmann and Stöckhert, 2001). Whereas the quartz microstructures in the associated metagranites (Trepmann and Stöckhert, 2003) are quite similar to the type C microstructure, the tectonic setting and the lithologies are very different. Yet, to our knowledge, it is the only estimate on the peak differential stress related to coseismic loading in the plastosphere at greenschist facies conditions.

The microstructures suggest that dislocation creep with localized recrystallization of quartz is dominating stress relaxation after coseismic glide-controlled deformation at peak differential stress. Therefore, a flow law for dislocation creep can be used to infer the time scale of stress and strain rate relaxation assuming temperatures between 300 °C and 350 °C and initial peak stresses of for example 300 MPa to 500 MPa. For these temperature and stress conditions, strain rates suggested by the flow law of Paterson and Luan (1990), Eq. (1), are on the order of 10^{-11} s^{-1} to 10^{-12} s^{-1}. Assuming a Maxwell rheology, the relaxation time (2) for these conditions is between ten to few hundred years (Fig. 7). Although strain rates during initial dislocation glide-controlled deformation might have been transiently higher, the rapidly relaxing strain rates cause that the overall amount of strain by dislocation glide and creep is low in comparison to the low-stress, high-strain rate dissolution-precipitation creep of the host rock.

5.5. Quartz veins and the seismic cycle

Quartz veins with a high ratio of aperture to length have been attributed to coseismic deformation and sealing during postseismic creep (Henderson and McCaig, 1996; Nüchter and Stöckhert, 2007, 2008; Birtel and Stöckhert, 2008). There, however, vein formation is monogenetic and crystallization occurred in an open cavity as opposed to the crack-seal microstructures, observed here (Fig. 2c–e). Fagereng et al. (2018) discussed the occurrence of quartz veins formed by dehydration reactions during metamorphism at 470–550 °C to reflect tremors along the subduction thrust interface. Dissolution-precipitation creep at high strain rates causing internal stress loading and thus multiple crack-seal episodes, is not contradictory to such scenarios, on the contrary, it might be triggered or at least amplified by seismic stress pulses. The quartz veins and local occurrence of high-stress deformation microstructures detected here can further be used for unravelling burial and exhumation histories, where the closer relation to the shear zones and faults in the study area needs to be discussed, which however is beyond the scope of this study.

6. Conclusions and summary

The quartz microstructures type A and type B in veins associated to boudins, kink bands and shear bands in metasediments (Figs. 1,

2, 3a–c) reflect episodes of cracking and sealing during dissolution-precipitation creep of the host rock at temperatures close to peak metamorphic conditions of around 350 °C. The time scale to cause cyclic cracking and sealing is assumed lower than the Maxwell relaxation time of the metasediments undergoing dissolution-precipitation creep at strain rates of 10^{-10} s^{-1} to 10^{-9} s^{-1}, which are a few tens to hundred years (Fig. 7). The generally low amount of strain accumulated by dislocation creep of quartz in the host rock indicates that bulk stresses stayed below a few tens of MPa at the given temperature conditions on a long term.

In some veins concordant or discordant to the foliation, the heterogeneous type C quartz microstructure is characterized by micro-shear zones, SWUE, sub-basal deformation lamellae and recrystallized grains restricted to high strain zones (Figs. 3d–f, 4–6). These microstructures indicate local and transient high-stress dislocation-glide controlled deformation (low-T plasticity, Peierls stress-controlled glide) and subsequent dislocation creep at relaxing stresses. The indicated stresses of a few hundred MPa are explained by fast (coseismic) stress-loading rates resulting from a seismic slip event in the overlying seismogenic layer, i.e. on the time scale of seconds to minutes (Fig. 7). Stress relaxation is controlled by dislocation creep at rapidly decaying strain rates from initially about 10^{-11} s^{-1} to 10^{-12} s^{-1} at time scales of tens to hundred years. The overall amount of strain by dislocation glide and creep is low in comparison to the low-stress, high-strain rate dissolution-precipitation creep of the host rock.

The study demonstrates that quartz microstructures are a powerful tool to distinguish different stress histories during deformation and to detect transient deformation caused by seismic activity.

Acknowledgments

This study was funded by the German research foundation (DFG Grant No. TR534/5-1). Two anonymous reviewers are gratefully acknowledged. Special acknowledgements go to Jens Nüchter, Bernhard Stöckhert, Gernold Zulauf, Wolfgang Dörr and Jochen Krahl for constructive discussions. We thank Markus Döblinger for help with TEM investigations at Ludwig-Maximilians University Munich, Department of Chemistry, and Namvar Jahanmehr and Michael Herrmann for preparation of thin sections.

References

Ague, J.J., 1994. Mass transfer during Barrovian metamorphism of pelites, south-central Connecticut; II, Channelized fluid flow and the growth of staurolite and kyanite. American Journal of Science 294, 1061–1134.
Ague, J.J., 1995. Deep crustal growth of quartz, kyanite and garnet into large-aperture, fluid-filled fractures, north-eastern Connecticut, USA. Journal of Metamorphic Geology 13, 299–314.
Birtel, S., Stöckhert, B., 2008. Quartz veins record earthquake-related brittle failure and short term ductile flow in the deep crust. Tectonophysics 457, 53–63.
Bons, P.D., Elburg, M.A., Gomez-Rivas, E., 2012. A review of the formation of tectonic veins and their microstructures. Journal of Structural Geology 43, 33–62.
Ceccato, A., Pennacchioni, G., Bestmann, M., 2017. Crystallographic control and texture inheritance duringmylonitization of coarse grained quartz veins. Lithos 290–291, 210–227.
Christie, J.M., Ardell, A.J., 1974. Substructures of deformation lamellae in quartz. Geology 2, 405–408.
Cox, S.F., Etheridge, M.A., 1983. Crack-seal fibre growth mechanisms and their significance in the development of oriented layer silicate microstructures. Tectonophysics 92, 147–170.
Drury, M.R., 1993. Deformation Lamellae in Metals and Minerals. Defects and processes in the solid state: Geoscience applications: McLaren volume. Elsevier, Amsterdam, The Netherlands, pp. 195–212.
Durney, D.W., Ramsay, J.G., 1973. Incremental strains measured by syntectonic crystal growth. In: De Jong, K.A., Scholten, R. (Eds.), Gravity and Tectonics. Wiley, New York, pp. 67–69.
Ellis, S., Beavan, J., Eberhart-Phillips, D., Stöckhert, B., 2006. Simplified models of the Alpine Fault seismic cycle: stress transfer in the mid-crust. Geophysical Journal International 166, 386–402.
Ellis, S., Stöckhert, B., 2004. Elevated stresses and creep rates beneath the brittle-ductile transition caused by seismic faulting in the upper crust. Journal of Geophysical Research Solid Earth 109. B05407.
Epting, M., Kudrass, H.-R., Leppig, U., Schäfer, A., 1972. Geologie der Talea Ori/Kreta. Neues Jahrbuch der Geologie und Paläontologie 141, 259–285.
Fagereng, Å., Diener, J.F.A., Meneghini, F., Harris, C., Kvadsheim, A., 2018. Quartz vein formation by local dehydration embrittlement along the deep, tremorgenic subduction thrust interface. Geology 46, 67–70.
Fagereng, Å., Sibson, R.H., 2010. Melange rheology and seismic style. Geology 38, 751–754.
Famin, V., Philippot, P., Jolivet, L., Agard, P., 2004. Evolution of hydrothermal regime along a crustal shear zone, Tinos Island, Greece. Tectonics 23. https://doi.org/10.1029/2003TC001509. B05407.
Fassoulas, C., Kilias, A., Mountrakis, D., 1994. Postnappe stacking extension and exhumation of high-pressure/low-temperature rocks in the island of Crete, Greece. Tectonics 13, 127–138.
Fisher, D.M., Brantley, S.L., 1992. Models of quartz overgrowth and vein formation: deformation and episodic fluid flow in an ancient subduction zone. Journal of Geophysical Research Solid Earth 97 (B13), 20043–20061.
Fisher, D.M., Brantley, S.L., Everett, M., Dzvonik, J., 1995. Cyclic fluid flow through a regionally extensive fracture network within the Kodiak accretionary prism. Journal of Geophysical Research Solid Earth 100 (B7), 12881–12894.
Fisher, D., Byrne, T., 1990. The character and distribution of mineralized fractures in the Kodiak Formation, Alaska: implications for fluid flow in an underthrust sequence. Journal of Geophysical Research Solid Earth 95 (B6), 9069–9080.
Henderson, I.H.C., McCaig, A.M., 1996. Fluid pressure and salinity variations in shear zone-related veins, central Pyrenees, France: implications for the fault-valve model. Tectonophysics 262, 321–348.
Hilgers, C., Dilg-Gruschinski, K., Urai, J.L., 2003. Microstructures grown experimentally from advective supersaturated solution and their implication for natural vein systems. Journal of Geochemical Exploration 78, 221–225.
Hilgers, C., Koehn, D., Bons, P.D., Urai, J.L., 2001. Development of crystal morphology during unitaxial growth in a progressively widening vein: II. Numerical simulations of the evolution of antitaxial fibrous veins. Journal of Structural Geology 23, 873–885.
Hilgers, C., Urai, J.L., 2002. Experimental study of syntaxial vein growth during lateral fluid flow in transmitted light: first results. Journal of Structural Geology 24, 1029–1043.
Hobbs, B.E., 1968. Recrystallization of single crystals of quartz. Tectonophysics 6, 353–401.
Hobbs, B.E., Ord, A., Teyssier, C., 1986. Earthquakes in the ductile regime? Pure and Applied Geophysics 124, 309–336.
Johnson, R.B., DeGraff, J.V., 1988. Principles of Engineering Geology. Wiley, p. 497 pp..
Jolivet, L., Goffé, B., Monié, P., Truffert-Luxey, C., Patriat, M., Bonneau, M., 1996. Miocene detachment in Crete and exhumation P-T-t paths of high-pressure metamorphic rocks. Tectonics 15, 1129–1153.
Kilian, R., Heilbronner, R., 2017. Analysis of crystallographic preferred orientations of experimentally deformed Black Hills Quartzite. Solid Earth 8, 1095–1117.
Kjøll, H.J., Viola, G., Menegon, L., Sørensen, B.E., 2015. Brittle-viscous deformation of vein quartz under fluid-rich lower greenschist facies conditions. Solid Earth 6, 681.
Kock, S., Martini, R., Reischmann, T., Stampfli, G., 2007. Detrital zircon and micro-palaeontological ages as new constraints for the lowermost tectonic unit (Talea Ori unit) of Crete, Greece. Palaeogeography Palaeoclimatology Palaeoecology 243, 307–321.
Küster, M., Stöckhert, B., 1999. High differential stress and sublithostatic pore fluid pressure in the ductile regime – microstructural evidence for short-term post-seismic creep in the Sesia Zone, Western Alps. Tectonophysics 303, 263–277.
Lloyd, G.E., 2004. Microstructural evolution in a mylonitic quartz simple shear zone: the significant roles of dauphine twinning and misorientation. In: Alsop, G.I., Holdsworth, R.E., McCaffrey, K.J.W., Hand, M. (Eds.), Flow Processes in Faults and Shear Zones. Geological Society London Special Publications, London, pp. 39–61.
Masuda, T., Shibutani, T., Igarashi, T., Kuriyama, M., 1989. Microboudin structure of piedmontite in quartz schists: a proposal for a new indicator of relative palaeo-differential stress. Tectonophysics 163, 169–180.
McClusky, S., Balassanian, S., Barka, A., et al., 2000. Global Positioning System constraints on plate kinematics and dynamics in the eastern Mediterranean and Caucasus. Journal of Geophysical Research 105, 5695–5719.
McLaren, A.C., Hobbs, B.E., 1972. Transmission electron microscope investigation of some naturally deformed quartzites. Flow and Fracture of Rocks 55–66.
McLaren, A.C., Turner, R.G., Boland, J.N., Hobbs, B.E., 1970. Dislocation structure of the deformation lamellae in synthetic quartz; a study by electron and optical microscopy. Contributions to Mineralogy and Petrology 29, 104–115.
Menegon, L., Piazolo, S., Pennacchioni, G., 2011. The effect of Dauphiné twinning on plastic strain in quartz. Contributions to Mineralogy and Petrology 161, 635–652.
Nollet, S., Urai, J.L., Bons, P.D., Hilgers, C., 2005. Numerical simulations of polycrystal growth in veins. Journal of Structural Geology 27, 217–230.
Nüchter, J.-A., Ellis, S., 2010. Complex states of stress during the normal faulting seismic cycle: role of midcrustal postseismic creep. Journal of Geophysical Research Solid Earth 115, B12411.
Nüchter, J.-A., Ellis, S., 2011. Mid-crustal controls on episodic stress field rotation around major reverse, normal and strike-slip faults. In: Fagereng, Å., Toy, V.G.,

Rowland, J.V. (Eds.), Geology of the Earthquake Source: A Volume in Honour of Rick Sibson, vol. 359. Geological Society London Special Publication, London, United Kingdom, pp. 187–201.
Nüchter, J.-A., Stöckhert, B., 2007. Vein quartz microfabrics indicating progressive evolution of fractures into cavities during postseismic creep in the middle crust. Journal of Structural Geology 29, 1445–1462.
Nüchter, J.A., Stöckhert, B., 2008. Coupled stress and pore fluid pressure changes in the middle crust: vein record of coseismic loading and postseismic stress relaxation. Tectonics 27, TC1007. https://doi.org/10.1029/2007TC002180.
Olson, J.E., 2003. Sublinear scaling of fracture aperture versus length: an exception or the rule? Journal of Geophysical Research 108.
Passchier, C.W., Trouw, R.A., 2005. Microtectonics, vol. 1. Springer Science & Business Media.
Platt, J., Vissers, R., 1980. Extensional structures in anisotropic rocks. Journal of Structural Geology 2, 397–410.
Paterson, M.S., Luan, F.C., 1990. Quartzite rheology under geological conditions. In: Knipe, R.J., Rutter, E.H. (Eds.), Deformation Mechanisms, Rheology and Tectonics, vol. 54. Geological Society Special Publication, pp. 299–307.
Pehl, J., Wenk, H.R., 2005. Evidence for regional Dauphiné twinning in quartz from the Santa Rosa mylonite zone in Southern California. A neutron diffraction study. Journal of Structural Geology 27, 1741–1749.
Peters, M., Herwegh, M., Paesold, M.K., Poulet, T., Regenauer-Lieb, K., Veveakis, M., 2016. Boudinage and folding as an energy instability in ductile deformation. Journal of Geophysical Research Solid Earth 121, 3996–4013. https://doi.org/10.1002/2016JB012801.
Poole, R.J., 2012. The Deborah and weissenberg numbers. The British Society of Rheology Rheology Bulletin 53, 32–39.
Rahl, J.M., Anderson, K.M., Brandon, M.T., Fassoulas, C., 2005. Raman spectroscopic carbonaceous material thermometry of low-grade metamorphic rocks: calibration and application to tectonic exhumation in Crete, Greece. Earth and Planetary Science Letters 240, 339–354.
Ramsay, J.G., 1980. The crack–seal mechanism of rock deformation. Nature 284, 135–139.
Ramsay, J.G., Huber, M.I., 1983. Techniques of Modern Structural Geology, vol. 1. Strain Analysis. Academic Press, London, 307pp.
Ranalli, G., 1995. Rheology of the Earth, second ed. Chapman & Hall, London, p. 416.
Richter, D., Kopp, K., 1983. Zur Tektonik der untersten geologischen Stockwerke auf Kreta. Monatsh 1983, 27–46. Neues Jahrbuch für Geologie.
Ring, U., Glodny, J., Will, T., Thomson, S., 2010. The Hellenic subduction system: high-pressure metamorphism, exhumation, normal faulting, and large-scale extension. Annual Review of Earth and Planetary Sciences 38, 45–76.
Scholz, C.H., 2002. The Mechanics of Earthquakes and Faulting. Cambridge University Press, Cambridge, p. 471.
Scholz, C.H., 1988. The brittle-plastic transition and the depth of seismic faulting. Geologische Rundschau 77, 319–328.
Sibson, R.H., 1977. Fault rocks and fault mechanisms. Journal of the Geological Society 133, 191–213.
Seidel, M., Seidel, E., Stöckhert, B., 2007. Tectono-sedimentary evolution of lower to middle Miocene half-graben basins related to an extensional detachment fault (western Crete, Greece). Terra Nova 19 (1), 39–47.
Seidel, E., Kreuzer, H., Harre, W., 1982. A late Oligocene/early Miocene high pressure belt in the external Hellenides. Geologisches Jahrbuch E 23, 165–206.
Stipp, M., Kunze, K., 2008. Dynamic recrystallization near the brittle-plastic transition in naturally and experimentally deformed quartz aggregates. Tectonophysics 448, 77–97.
Stipp, M., Tullis, J., 2003. The recrystallized grain size piezometer for quartz. Geophysical Research Letters 30, 2088. https://doi.org/10.1029/2003GL018444.
Stöckhert, B., 2002. Stress and deformation in subduction zones: insight from the record of exhumed metamorphic rocks. In: De Meer, S., Drury, M.R., De Bresser, J.H.P., Pennock, G.M. (Eds.), Deformation Mechanisms, Rheology and Tectonics: Current Status and Future Perspectives, vol. 200. Geological Society London Special Publications, London, pp. 255–274.
Stöckhert, B., Wachmann, M., Küster, M., Bimmermann, S., 1999. Low effective viscosity during high pressure metamorphism due to dissolution precipitation creep: the record of HP-LT metamorphic carbonates and siliciclastic rocks from Crete. Tectonophysics 303, 299–319.
Theye, T., Seidel, E., Vidal, O., 1992. Carpholite, sudoite, and chloritoid in low-grade high-pressure metapelites from Crete and the Peloponnese, Greece. European Journal of Mineralogy 4 (3), 487–507.
Thomson, S.N., Stöckhert, B., Brix, M.R., 1998. Thermochronology of the high-pressure metamorphic rocks of Crete, Greece: implications for the speed of tectonic processes. Geology 26, 259–262.
Thomson, S.N., Stöckhert, B., Brix, M.R., 1999. Miocene High-pressure Metamorphic Rocks of Crete, Greece: Rapid Exhumation by Buoyant Escape, vol. 154. Geological Society, London, Special Publications, pp. 87–107.
Trepmann, C.A., Stöckhert, B., Dorner, D., Küster, M., Röller, K., Moghadam, R.H., 2007. Simulating coseismic deformation of quartz in the middle crust and fabric evolution during postseismic stress relaxation – an experimental study. Tectonophysics 442, 83–104.
Trepmann, C.A., Stöckhert, B., 2001. Mechanical twinning of jadeite - an indication of synseismic loading beneath the brittle-ductile transition. International Journal of Earth Sciences 90, 4–13.
Trepmann, C.A., Stöckhert, B., 2003. Quartz microstructures developed during non-steady state plastic flow at rapidly decaying stress and strain rate. Journal of Structural Geology 25, 2035–2051.
Trepmann, C.A., Hsu, C., Hentschel, F., Döhler, K., Schneider, C., Wichmann, V., 2017. Recrystallization of quartz after low-temperature plasticity - the record of stress relaxation below the seismogenic zone. Journal of Structural Geology 95, 77–92. https://doi.org/10.1016/j.jsg.2016.12.004.
Trepmann, C.A., Lenze, A., Stöckhert, B., 2010. Static recrystallization of vein quartz pebbles in a high-pressure–low-temperature metamorphic conglomerate. Journal of Structural Geology 32, 202–215.
Trepmann, C.A., Stöckhert, B., 2009. Microfabric of folded quartz veins in metagreywackes: dislocation creep and subgrain rotation at high stress. Journal of Metamorphic Geology 27, 555–570.
Trepmann, C.A., Stöckhert, B., 2013. Short-wavelength undulatory extinction in quartz recording coseismic deformation in the middle crust – an experimental study. Solid Earth 4, 263–276.
Urai, J.L., Williams, P.F., Van Roermund, H.L.M., 1991. Kinematics of crystal growth in syntectonic fibrous veins. Journal of Structural Geology 13, 823–836.
Van Daalen, M., Heilbronner, R., Kunze, K., 1999. Orientation analysis of localized shear deformation in quartz fibres at the brittle–ductile transition. Tectonophysics 303, 83–107.
Vermilye, J.M., Scholz, C.H., 1995. Relations between vein length and aperture. Journal of Structural Geology 238, 423–434.
Vernooij, M.G.C., Langenhorst, F., 2005. Experimental reproduction of tectonic deformation lamellae in quartz and comparison to shock-induced planar deformation features. Meteoritecs and Planetary Science 40, 1353–1361.
Wald, D.J., Heaton, T.H., 1994. Spatial and temporal distribution of slip for the 1992 Landers, California, earthquake. Bulletin of the Seismological Society of America 84, 668–691.
Wassmann, S., Stöckhert, B., 2013. Rheology of the plate interface—dissolution precipitation creep in high pressure metamorphic rocks. Tectonophysics 608, 1–29.
Wenk, H.R., Janssen, C., Kenkmann, T., Dresen, G., 2011. Mechanical twinning in quartz: shock experiments, impact, pseudotachylites and fault breccias. Tectonophysics 510, 69–79.
Wenk, H.R., Rybacki, E., Dresen, G., Lonardelli, I., Barton, N., Franz, H., Gonzalez, G., 2006. Dauphiné twinning and texture memory in polycrystalline quartz. Part 1: experimental deformation of novaculite. Physics and Chemistry of Minerals 33, 667.
White, J.C., 1996. Transient discontinuities revisited: pseudotachylyte, plastic instability and the influence of low pore fluid pressure on deformation processes in the mid-crust. Journal of Structural Geology 18, 1471–1486.
White, J.C., 2012. Paradoxical pseudotachylyte - fault melt outside the seismogenic zone. Journal of Structural Geology 38, 11–20.
White, S., 1973. Syntectonic recrystallization and texture development in quartz. Nature 244, 276–278.
White, S., 1977. Geological significance of recovery and recrystallization processes in quartz. Tectonophysics 39, 143–170.
Zulauf, G., Dörr, W., Krahl, J., Lahaye, Y., Chatzaras, V., Xypolias, P., 2016. U–Pb zircon and biostratigraphic data of high-pressure/low-temperature metamorphic rocks of the Talea Ori: tracking the Paleotethys suture in central Crete, Greece. International Journal of Earth Sciences 105, 1901–1922.